RSC Advances

PAPER

View Article Online
View Journal | View Issue

Cite this: *RSC Adv.*, 2015, **5**, 101932

Synthesis, molecular structure and electrochemical properties of nickel(II) benzhydrazone complexes: influence of ligand substitution on DNA/protein interaction, antioxidant activity and cytotoxicity†

Ramasamy Raj Kumar and Rengan Ramesh*

Received 22nd September 2015
Accepted 10th November 2015

DOI: 10.1039/c5ra19530f

www.rsc.org/advances

A series of new nickel(II) benzhydrazone complexes having the general formula $[Ni(L)_2]$ (where L = thiophene aldehyde benzhydrazone) have been synthesized *via* the reaction of $Ni(OAc)_2 \cdot 4H_2O$ with 2 equivalents of benzhydrazone ligands in a DMF/ethanol medium. The complexes have been characterized by analytical, spectral (FT-IR, UV-vis, NMR and ESI-mass) and single-crystal X-ray crystallography methods. All the complexes exhibit quasi-reversible one-electron reduction responses (Ni^{II}–Ni^{I}) within the $E_{1/2}$ range from −0.71 to −0.77 V *versus* SCE. The structure of one of the complexes has been determined by a single-crystal X-ray diffraction study, which shows that coordination of the benzhydrazone ligands to the nickel occurs *via* azomethine nitrogen and imidolate oxygen atoms as monobasic bidentate donors with two units of the ligand in a square-planar geometry. The DNA-binding interactions of the complexes with calf thymus DNA have been investigated by absorption, emission, electrochemical, circular dichroism and viscosity measurements, which revealed that the complexes could interact with DNA *via* intercalation. The protein-binding interactions of the complexes with BSA were investigated by UV-vis, fluorescence and synchronous fluorescence methods, which indicated that stronger binding of the complexes with BSA and a static quenching mechanism was observed. Moreover, the potential for free-radical scavenging of all the complexes was also determined using DPPH, hydroxyl and nitric oxide radicals under *in vitro* conditions. Furthermore, the cytotoxicity of all the complexes was examined *in vitro* on the human cervical cancer cell line HeLa, MCF-7 and the normal mouse embryonic fibroblast cell line NIH-3T3 under identical conditions and they exhibited good IC_{50} values. These values were further supported by a neutral red uptake assay using HeLa cell lines. AO-EB/DAPI staining assays and flow cytometry analysis revealed that the complexes induce cell death only by apoptosis.

Introduction

The interaction of metal complexes with DNA has long been a subject of great interest in relation to the development of new reagents for biotechnology and medicine.[1–3] A number of biological experiments have also revealed that DNA is the main intracellular target of anticancer drugs due to the interaction between small molecules and DNA, which can cause damage to DNA in cancer cells, prevent the division of cancer cells and result in cell death.[4] The accidental discovery of the antitumor properties of cisplatin by Rosenberg *et al.*[5,6] was followed by one of the most impressive drug success stories ever and significant improvements to cancer therapy. In addition to cisplatin, several platinum complexes (carboplatin, oxaliplatin, nedaplatin and lobaplatin) have been approved for current tumour therapy. Complexes of ruthenium, titanium, and gallium have already been tested in clinical phase I and phase II studies.[7,8] Preclinical research also involves metal complexes containing other non-platinum metals (*e.g.*, iron, cobalt, and gold).[9]

The interactions of metal complexes with serum albumins have received much attention in the scientific community *via* studying the pharmacodynamics and structure–activity relationships of antitumor metallopharmaceuticals.[10] Serum albumins are the most abundant proteins in plasma and have many physiological functions.[11–13] In particular, they contribute to the control of osmotic blood pressure and the maintenance of blood pH.[14] BSA is the most well-studied serum albumin due to its structural resemblance to human serum albumin (HSA).

Free radicals inside the human body play a pathogenic role in most chronic degenerative diseases, including inflammatory,

School of Chemistry, Bharathidasan University, Tiruchirappalli – 620 024, Tamil Nadu, India. E-mail: ramesh_bdu@yahoo.com; rrameshbdu@gmail.com; Fax: +91-431-2407045/2407020; Tel: +91-431-2407053

† Electronic supplementary information (ESI) available: UV-vis, ESI-mass and cyclic voltammograms of the complexes. CCDC 1032855. For ESI and crystallographic data in CIF or other electronic format see DOI: 10.1039/c5ra19530f

cancer, autoimmune, cardiovascular and neurodegenerative diseases and aging.[15–18] Free radicals can adversely affect lipids, proteins and DNA and have been implicated in the aging process and in a number of human diseases. Antioxidants are capable of neutralising these reactive species in terms of prevention, interception and damage repair.[19,20]

Hydrazones are an important class of ligands with interesting ligation properties due to the presence of several coordination sites[21] and are widely applied in the fields of medicines, insecticides and analytical reagents due to their superior bioactivity.[22] The hydrazone unit offers a number of interesting features such as a degree of rigidity, a conjugated π system and a NH unit that readily participates in hydrogen bonding and may be a site of protonation–deprotonation. Some hydrazone analogs have been investigated as potential oral iron-chelating drugs for the treatment of genetic disorders such as thalassemia and have also been proposed as possible metal-chelating agents for treating neurodegenerative disorders such as Alzheimer's disease.[23–25] Hydrazone ligands create an environment similar to that present in biological systems, usually by coordination through oxygen and nitrogen atoms. In this respect, the formation of metal complexes plays a substantial role in enhancing their biological activity.

Although this was not understood until the 1970s, nickel plays important roles as a catalytic center in both redox and non-redox enzymes, wherein it has important consequences in human health (*e.g.*, urease), energy science (*e.g.*, hydrogenase), and environment (*e.g.*, carbon monoxide dehydrogenases).[26] Nickel(II) compounds, which can be reversibly reduced to nickel(I) species, have attracted attention as models of redox-active nickel-containing enzymes[27] and as electrocatalysts.[28] Complementing their natural biochemical functions, complexes of nickel also display pharmacological potential. Nickel(II) complexes are regarded as some of the most promising alternatives to the traditional cisplatin as anticancer drugs. This idea is supported by an extensive number of research articles that describe the synthesis, DNA-binding and cytotoxic activities of numerous nickel(II) complexes.[29–31] The synthesis, structure, DNA-binding properties and antioxidant activity of a nickel(II) complex with bis(*N*-allylbenzimidazol-2-ylmethyl)benzylamine have been reported.[32] The synthesis, characterisation and *in vitro* pharmacological evaluation of new water-soluble Ni(II) complexes of 4N-substituted thiosemicarbazones of 2-oxo-1,2-dihydroquinoline-3-carboxaldehyde have been described.[33] The synthesis, structure and biological activity of nickel(II) complexes with mefenamat and nitrogen-donor ligands have been reported.[34] Variations in the biomolecular interactions of nickel(II) hydrazone complexes upon tuning the hydrazide fragment have been reported.[35]

Therefore, considerable attempts are being made to research the interaction of nickel(II) complexes with DNA and their cytotoxic activities. Based on the abovementioned facts and considering the role and activity of nickel and its complexes in biological systems, along with the significance of hydrazones in medicine, we report in this study a systematic study of the synthesis, structure and electrochemical properties of nickel(II) complexes containing thiophene aldehyde benzhydrazone ligands and their interactions with DNA/protein, antioxidant activity and cytotoxicity. In addition, the effect of substituents in nickel(II) complexes on the abovementioned properties is also studied in detail.

Experimental section

Materials and instrumentation

Nickel(II) acetate tetrahydrate, thiophene-2-carboxaldehyde and benzhydrazide derivatives were purchased from Merck and Aldrich Chemicals and used as received. Solvents were dried and freshly distilled prior to use. Calf thymus DNA (CT-DNA) and ethidium bromide (EtBr) were purchased from Sigma-Aldrich Chemicals and used as received. Bovine serum albumin (BSA) was purchased from Himedia. 3-(4,5-Dimethylthiazol-2-yl)-2,5-diphenyltetrazolium bromide (MTT) was purchased from Sigma-Aldrich and used as received. Human cervical cancer cells and MCF-7 human breast cancer cells were obtained from the National Centre for Cell Science (NCCS), Pune, India. The annexin V-FITC kit (APOAF-20TST) from Sigma-Aldrich was utilized according to the instructions from the manufacturer. All other chemicals and reagents used for biological studies were of high-quality biological grade. Elemental analyses were performed on a Vario EL III CHNS elemental analyser. Melting points were measured with an electrical instrument and are uncorrected. Infrared spectra were obtained in KBr pellets with a JASCO 200 Plus spectrometer. NMR spectra were obtained in DMSO-d_6 for the ligands and complexes with a Bruker 400 MHz instrument using TMS as the internal reference. Mass spectrometric analysis was performed using the ESI technique on a Waters Q-TOF Micro mass spectrometer for all these complexes in solution in DMF. Electronic spectroscopy was performed with a Cary 300 Bio (Varian) spectrophotometer using cuvettes with a path length of 1 cm. Emission intensity measurements were carried out using a Jasco FP-6500 spectrofluorometer. Circular dichroism spectra were obtained using a JASCO J-810 spectropolarimeter equipped with a Peltier temperature-control device at room temperature with a quartz cell with a path length of 1 cm. Results for each sample solution were the average of three accumulations using a scan speed of 500 nm min^{-1} at a response time of 1 s. Viscosity measurements were carried out on a Schott Geräte AVS 310 viscometer at 29 $\pm$ 0.1 °C in a thermostatic water bath. The supporting electrolyte tetrabutylammonium perchlorate (TBAP) was purchased from Aldrich and dried in vacuum prior to use. Electrochemical measurements were made using a CH instrument using a glassy carbon working electrode and 0.05 M [(n-$C_4H_9)_4N$](ClO_4) (TBAP) as the supporting electrolyte. All potentials were referenced to the saturated calomel electrode (SCE) and the solutions were purged with N_2 before each set of experiments.

Preparation of benzhydrazone ligands

Monobasic bidentate benzhydrazone ligands were prepared by a reported procedure.[36] To a stirred ethanolic solution (10 mL) of 4-substituted benzhydrazide (68–85 mg, 5 mmol), an ethanolic (10 mL) solution of thiophene-2-aldehyde (0.46 mL, 56–63 mg, 5 mmol) was added dropwise. The reaction mixture was

refluxed for 3 h and the solution concentrated to 5 mL and cooled to room temperature. The solid that was formed was filtered, washed with cold methanol (5 mL) and dried in air.

Benzoic acid thiophene-2-ylmethylene-hydrazide (HL1). Colour: cream; yield: 87%; mp: 150 °C; anal. calc. for $C_{12}H_{10}N_2OS$ (230.29 g mol^{-1}): C, 62.58; H, 4.37; N, 12.16; S, 13.92. Found: C, 62.53; H, 4.40; N, 12.10; S, 13.96. IR (KBr, cm^{-1}): 3254 s $\nu_{(N-H)}$, 1644 s $\nu_{(C=N)}$ + $\nu_{(C=O)}$. ^{1}H NMR (400 MHz, DMSO-d$_6$) δ (ppm): 11.8 (s, 1H, NH), 8.7 (s, 1H, CH=N), 7.2–8.0 (m, 8H, aromatic). UV-vis (DMF): 265, 322 nm.

4-Chlorobenzoic acid thiophene-2-ylmethylene-hydrazide (HL2). Colour: cream; yield: 86%; mp: 156 °C; anal. calc. for $C_{12}H_9ClN_2OS$ (264.73 g mol^{-1}): C, 54.44; H, 3.42; N, 10.58; S, 12.11. Found: C, 54.48; H, 3.46; N, 10.60; S, 12.14. IR (KBr, cm^{-1}): 3280 s $\nu_{(N-H)}$, 1639 s $\nu_{(C=N)}$ + $\nu_{(C=O)}$. ^{1}H NMR (400 MHz, DMSO-d$_6$) δ (ppm): 11.9 (s, 1H, NH), 8.7 (s, 1H, CH=N), 7.2–8.0 (m, 7H, aromatic). UV-vis (DMF): 268, 324 nm.

4-Bromobenzoic acid thiophene-2-ylmethylene-hydrazide (HL3). Colour: cream; yield: 84%; mp: 158 °C; anal. calc. for $C_{12}H_9BrN_2OS$ (309.18 g mol^{-1}): C, 46.61; H, 2.93; N, 9.06; S, 10.37. Found: C, 46.60; H, 2.98; N, 9.05; S, 10.25. IR (KBr, cm^{-1}): 3296 s $\nu_{(N-H)}$, 1636 s $\nu_{(C=N)}$ + $\nu_{(C=O)}$. ^{1}H NMR (400 MHz, DMSO-d$_6$) δ (ppm): 11.9 (s, 1H, NH), 8.7 (s, 1H, CH=N), 7.1–7.9 (m, 7H, aromatic). UV-vis (DMF): 268, 323 nm.

4-Methoxybenzoic acid thiophene-2-ylmethylene-hydrazide (HL4). Colour: cream; yield: 87%; mp: 162 °C; anal. calc. for $C_{13}H_{12}N_2O_2S$ (260.31 g mol^{-1}): C, 59.98; H, 4.64; N, 10.76; S, 12.31. Found: C, 60.01; H, 4.63; N, 12.34; S, 12.29. IR (KBr, cm^{-1}): 3272 s $\nu_{(N-H)}$, 1642 s $\nu_{(C=N)}$ + $\nu_{(C=O)}$. ^{1}H NMR (400 MHz, DMSO-d$_6$) δ (ppm): 11.7 (s, 1H, NH), 8.7 (s, 1H, CH=N), 7.2–8.9 (m, 7H, aromatic), 3.8 (s, 3H, OCH_3). UV-vis (DMF): 268, 324 nm.

Synthesis of new square planar nickel(II) benzhydrazone complexes

All reactions were carried out under anhydrous conditions and the new nickel(II) complexes were prepared according to the following procedure.[37] A hot solution of $Ni(CH_3COO)_2 \cdot 4H_2O$ (1 mmol) in ethanol was added to a boiling solution of the benzhydrazone ligands (2 mmol) (HL1–HL4) in DMF. The reaction mixtures were heated to reflux for 5 h. An orange-colored mononuclear complex $[Ni(L)_2]$ was precipitated. The solid was separated by filtration, washed with ethanol and diethyl ether then dried under vacuum.

$[Ni(L1)_2]$ (1)

Color: orange; yield: 91.9%; mp: 328 °C; anal. calc. for $C_{24}H_{18}N_4S_2O_2Ni$ (517.25 g mol^{-1}): C, 55.72; H, 3.50; N, 10.83; S, 12.39. Found: C, 55.80; H, 3.59; N, 10.88; S, 12.38. IR (KBr, cm^{-1}): 1526 s $\nu_{(C=N-N=C)}$, 1242 s $\nu_{(C-O)}$. UV-vis in DMF: $\lambda\varepsilon_{max}$/nm (ε_{max}/dm^3 mol^{-1} cm^{-1}) 268(60, 470) (intraligand transition), 361(10 326) (LMCT), 424(1965) (forbidden d → d transition). ESI-MS: *m*/*z* 522.85.

$[Ni(L2)_2]$ (2)

Color: orange; yield: 89%; mp: 340 °C; anal. calc. for $C_{24}H_{16}Cl_2N_4S_2O_2Ni$ (586.14 g mol^{-1}): C, 49.17; H, 2.75; N, 9.55; S, 10.94. Found: C, 49.22; H, 2.68; N, 9.50; S, 10.98. IR (KBr, cm^{-1}): 1583 s $\nu_{(C=N-N=C)}$, 1238 s $\nu_{(C-O)}$. UV-vis in DMF: λ_{max}/nm (ε_{max}/dm^3 mol^{-1} cm^{-1}) 266(86, 760) (intraligand transition), 363(14 308) (LMCT), 424(1086) (forbidden d → d transition). ESI-MS: *m*/*z* 592.57.

$[Ni(L3)_2]$ (3)

Color: orange; yield: 88.49%; mp: 344 °C; anal. calc. for $C_{24}H_{16}Br_2N_4S_2O_2Ni$ (675.05 g mol^{-1}): C, 42.70; H, 2.38; N, 8.29; S, 9.50. Found: C, 42.62; H, 2.39; N, 8.20; S, 9.49. IR (KBr, cm^{-1}): 1578 s $\nu_{(C=N-N=C)}$, 1240 s $\nu_{(C-O)}$. UV-vis in DMF: λ_{max}/nm (ε_{max}/dm^3 mol^{-1} cm^{-1}) 265(80, 720) (intraligand transition), 365(11 252) (LMCT), 426(2559) (forbidden d → d transition). ESI-MS: *m*/*z* 682.70.

$[Ni(L4)_2]$ (4)

Color: orange; yield: 97.05%; mp: 352 °C; anal. calc. for $C_{26}H_{22}N_4S_2O_4Ni$ (574.41 g mol^{-1}): C, 54.36; H, 3.86; N, 9.75; S, 11.16. Found: C, 54.30; H, 3.83; N, 9.78; S, 11.14. IR (KBr, cm^{-1}): 1520 s $\nu_{(C=N-N=C)}$, 1250 s $\nu_{(C-O)}$. UV-vis in DMF: λ_{max}/nm (ε_{max}/dm^3 mol^{-1} cm^{-1}) 272(80, 470) (intraligand transition), 367(11 187) (LMCT), 422(2422) (forbidden d → d transition). ESI-MS: *m*/*z* 577.48.

X-ray crystallography

Single crystals of complex **4** that were suitable for X-ray diffraction analysis were grown by slow evaporation of solutions of the complex in dimethylformamide at room temperature. Data collection was carried out using a Bruker SMART APEX II single-crystal X-ray diffractometer using monochromated MoK_α radiation (λ = 0.71073 Å). Absorption corrections were performed by a multi-scan method using the SADABS software.[38] Corrections were made for Lorentz and polarization effects. Structures were solved by SIR92 and refined by full-matrix least squares on F^2 using SHELXL 97.[39] All non-hydrogen atoms were refined anisotropically and the hydrogen atoms in these structures were located *via* the difference Fourier map and constrained to ideal positions in the refinement procedure. The unit cell parameters were determined by the method of difference vectors using reflections scanned from three different zones of the reciprocal lattice. Intensity data were measured using ω and φ scans with a frame width of 0.5°. Frame integration and data reduction were performed using the Bruker SAINT-Plus (version 7.06a) software.[40] The crystal structure and structure refinement parameters for the complex are given in Table 1.

DNA binding studies

Experiments involving the binding of compounds to CT-DNA were performed in double-distilled water with Tris (5 mM) and sodium chloride (50 mM) and the pH was adjusted to 7.2 with hydrochloric acid. A solution of CT-DNA in the buffer gave a ratio of UV absorbance of about 1.9 at 260 and 280 nm, which suggested that the DNA was sufficiently free from protein. The concentration per nucleotide was determined by electronic

Table 1 Crystal data and structure refinement of complex 4

Empirical formula	$C_{26}H_{22}N_4O_4S_2Ni$
Formula weight	577.29
Colour	Orange
Temperature (K)	296(2)
Wavelength (Å)	0.71073
Crystal system	Monoclinic
Space group	$P2_1/c$
a (Å)	13.5191(10)
b (Å)	5.4599(4)
c (Å)	18.3237(14)
α (°)	90.00
β (°)	108.169(4)
γ (°)	90.00
Volume (Å^3)	1285.09(17)
Z	2
D_{cal} (mg m^{-3})	1.431
Absorption coefficient (mm^{-1})	1.012
F(000)	532
Crystal size (mm)	0.54 × 0.09 × 0.09
Theta range (°)	1.59–30.39
Limiting indices	$-19 \le h \le 19$
	$-7 \le k \le 4$
	$-25 \le l \le 26$
Reflections collected	12 482
Independent reflections	3830
Data/restraints/parameters	3830/0/71
Goodness-of-fit (GOF) on F^2	1.041
Final R indices [$I > 2\sigma(I)$]	$R_1 = 0.0545$, w$R_2 = 0.1512$
R indices (all data)	$R_1 = 0.1151$, w$R_2 = 0.1159$
R_{int}	0.0463
Largest diff. peak and hole eA^{-3}	0.656 and −0.778

spectroscopy using a molar extinction coefficient of 6600 M^{-1} cm^{-1} at 260 nm. The complexes were dissolved in a combined solvent of 5% DMF and 95% Tris–HCl buffer for all experiments. A stock solution of CT-DNA was stored at 277 K and used after no more than 4 days. Electronic absorption titration experiments were performed by keeping a fixed concentration of the metal complex constant (25 μM) and varying the nucleotide concentration (0–60 μM). However, when obtaining the absorption spectra, equal amounts of DNA were added to both complex and reference solutions to eliminate the absorbance of DNA itself. Samples were equilibrated before obtaining each spectrum.

Further support for the binding of complexes to DNA *via* intercalation was obtained using fluorescence spectral techniques in order to find out whether a complex can displace EB from a DNA–EB complex. Ethidium bromide displacement experiments were carried out by adding solutions of the complexes to a Tris–HCl buffer solution (pH 7.2) of a DNA/EB mixture. DNA was pretreated with ethidium bromide at a [DNA]/[EB] ratio of 10 for 30 min at 27 °C, then a test solution was added to this mixture of EB–DNA and the change in fluorescence intensity was measured. The excitation wavelength was fixed at 545 nm for EB bound to DNA. Emissions were recorded with increasing concentrations of nickel(II) complexes and the emission range was adjusted before measurements. Metal complexes (0–60 μM) were then added to the mixture and their effect on the emission intensity was measured.

Cyclic voltammetry

Electrochemical studies were performed on a CH Instruments electrochemical analyser and the experiments were carried out in a three-electrode system comprising a glassy carbon working electrode, a platinum wire auxiliary/counter electrode and a saturated calomel electrode (SCE), which was used as the reference electrode. Cyclic voltammograms of the complexes were recorded in DMF solutions and buffer (5 mM Tris–HCl/50 mM NaCl, pH 7.2) solutions at a scan rate of 100 mV s^{-1}. TBAP and buffer solution were the supporting electrolytes. Oxygen was eliminated by purging the solutions with pure nitrogen gas, which had been previously saturated with solvent vapours. The electrode surfaces were freshly polished with alumina powder and washed with double-distilled water after each polishing step. All electrochemical measurements were performed at 25.0 ± 0.2 °C.

Circular dichroism

Circular dichroism is a useful technique for determining how the conformation of a CT-DNA chain is altered by a bound complex. A solution of CT-DNA displays a positive band (275 nm) from base-stacking interactions and a negative band (245 nm) from the right-handed helicity of DNA.[41] Conformational changes were measured upon the addition of complexes (20 μM) at a DNA concentration of 60 μM in a Tris–HCl buffer medium. The spectra of control DNA and the complexes were monitored from 220 to 320 nm. Classical intercalation reactions tend to increase the intensities of both bands due to strong base-stacking interactions of stable DNA conformations (right-handed B conformations of CT-DNA), whereas simple groove binding and electrostatic interactions with small molecules yield small perturbations or no perturbation in the base-stacking and helicity bands.[42]

Viscosity experiments

Viscosity experiments were performed using an Ubbelohde-type viscometer at a constant temperature of 29.0 ± 0.1 °C in a thermostatic water bath. Calf thymus DNA sample solutions were prepared by sonication in order to minimize complexities arising from the flexibility of DNA.[43] CT-DNA solutions (5 μM) were titrated with nickel(II) benzhydrazone complexes (0.5–5 μM), monitoring the variation in the viscosity in each case. The flow time was measured with a digital stopwatch; each sample was measured at least three times and an average flow time was calculated. Data are presented as $(\eta - \eta_o)^{1/3}$ *versus* the binding ratio, where η is the viscosity of DNA in the presence of the complex and η_o is the viscosity of DNA alone. Relative viscosity values were determined according to the equation $\eta = (t - t_o)/t_o$, where t_o is the total flow time for the buffer and t is the flow time that was observed for DNA in the presence and absence of the complex.[44]

Protein binding studies

The protein-binding interactions of nickel(II) hydrazone complexes with bovine serum albumin (BSA) were investigated

using fluorescence spectra, which were obtained with an excitation wavelength of 280 nm and an emission wavelength of 345 nm corresponding to those of free bovine serum albumin (BSA). The excitation and emission slit widths and scan rates were maintained at a constant for all experiments. Samples were thoroughly degassed using pure nitrogen gas for 15 minutes using quartz cells ($4 \times 1 \times 1$ cm) with high-vacuum Teflon stopcocks. Stock solutions of BSA were prepared in 50 mM phosphate buffer (pH 7.2) and stored in the dark at 4 °C for additional use. Concentrated stock solutions of metal complexes were prepared by dissolving them in DMF : phosphate buffer (5 : 95) and diluted suitably with phosphate buffer to obtain appropriate concentrations. A 2.5 mL solution of BSA (1 μM) was titrated by consecutive additions of a 25 μL stock solution of a complex (10^{-3} M) using a micropipette. Synchronous fluorescence spectra were also obtained using the same concentrations of BSA and complexes as mentioned above with two different values of $\Delta\lambda$ (difference between the excitation and emission wavelengths of BSA) such as 15 and 60 nm.

Protein cleavage experiments

Protein cleavage experiments were performed by incubating BSA (20 μM) with **1–4** in Tris–HCl buffer for 4 h at 37 °C according to the literature.[45] The samples were dissolved in a loading buffer (24 μL) containing SDS (7% w/v), glycerol (4% v/v), Tris–HCl buffer (50 mM, pH 7.2), mercaptoethanol (2% v/v) and bromophenol blue (0.01% w/v). The protein solutions were then denatured by heating to boil for 3 min. The samples were then loaded onto a 3% polyacrylamide (stacking) gel. Gel electrophoresis was carried out beginning at 60 V until the dye passed into the separating gel (12% polyacrylamide) from the stacking (3%) gel, followed by setting the voltage to 110 V for 1.5 h. Staining was performed with a Coomassie Brilliant Blue R-250 solution (acetic acid–methanol–water = 1 : 2 : 7 v/v) and destaining was carried out with a water–methanol–acetic acid mixture (5 : 4 : 1 v/v) for 4 h. The gels, after destaining, were scanned with a PrecisionScan LTX scanner and the images were further processed using the Adobe Photoshop 7.0 software package.

Antioxidant activity

The DPPH (2,2-diphenyl-1-picrylhydrazyl) radical-scavenging activity of the compounds was measured according to the method described by Blois.[46] The DPPH radical is a stable free radical having a λ_{max} of 517 nm. Various concentrations (10–50 μM) of the test compounds were added to a solution of DPPH (125 μM, 2 mL) in methanol and the final volume was made up to 4 mL with double-distilled water. The solution was incubated at 37 °C for 30 min in the dark. The decrease in the absorbance of DPPH was measured at 517 nm. The same experiment carried out without the test compounds served as a control.

Hydroxyl radicals that were produced by the Fe^{3+}/ascorbic acid system were detected according to the method of Nash.[47] The detection of hydroxyl radicals was carried out by measuring the amount of formaldehyde that was produced from an oxidation reaction with DMSO. Formaldehyde produced was detected spectrophotometrically at 412 nm. A mixture of 1.0 mL iron–EDTA solution (ferrous ammonium sulphate (0.331 mM) and EDTA (0.698 mM)), 0.5 mL EDTA solution (0.048 mM) and 1.0 mL DMSO (10.08 mM DMSO (v/v) in 0.1 M phosphate buffer, pH 7.4) was sequentially added to test tubes containing the test compounds at different concentrations in the range of 10–50 μM. The reaction mixture contained EDTA (0.1 mM), Fe^{3+} (167 μM), DMSO (33 mM) in phosphate buffer (50 mM, pH 7.4), and the tested compounds at various concentrations in the range of 10–50 μM. The reaction was initiated by adding 0.5 mL ascorbic acid (1.25 mM) and incubated at 80–90 °C for 15 min in a water bath. After incubation, the reaction was terminated by the addition of 1.0 mL ice-cold trichloroacetic acid (TCA) (107 mM). Subsequently, 3.0 mL Nash reagent was added to each tube, which was left at room temperature for 15 min. The reaction mixture without the sample was used as a control. The intensity of the colour that was formed was measured spectrophotometrically at 412 nm against a reagent blank.

Nitric oxide (NO) radical-scavenging activity was determined based on the reported method, in which sodium nitroprusside in an aqueous solution at physiological pH spontaneously generates nitric oxide, which interacts with oxygen to produce nitrate ions that can be estimated using the Griess reagent.[48] For this experiment, sodium nitroprusside (10 mM) in phosphate buffered saline was mixed with the test compounds at different concentrations in the range of 10–50 μM and incubated at room temperature for 150 min. The reaction mixture without the sample but with equivalent amount of solvent served as a control. After the incubation period, 0.5 mL Griess reagent containing sulphanilamide (5.8 mM), H_3PO_4 (20 mM) and *N*-(1-naphthyl)ethylenediamine dihydrochloride (0.39 mM) were added and mixed before standing for 30 min at 25 °C. The absorbance of the pink-coloured chromophore that was formed during diazotization was measured at 546 nm.

For the abovementioned three assays, all tests were run in triplicate and various concentrations of the complexes were used to establish a concentration at which the complexes displayed around 50% activity. The percentage activity was calculated using the formula: % suppression ratio = $[(A_o - A_c)/A_o] \times 100$, where A_o and A_c represent the absorbance in the absence and presence of the test compounds, respectively. The concentration that corresponds to 50% activity (IC_{50}) can be calculated using the percentage activity.

In vitro anticancer activity: maintenance of cell lines

Cell viability was evaluated by the 3-(4,5-dimethylthiazol-2-yl)-2,5-diphenyltetrazolium bromide (MTT) assay, which determines the metabolic activity of mitochondrial cells.[49] Cells were plated in a growth medium at a density of 5000 cells per well in 96 flat-bottomed well plates at a plating density of 10 000 cells per well and incubated to allow cell attachment at 37 °C under conditions of 5% CO_2, 95% air and 100% relative humidity. After 24 h, the cells were treated with serial concentrations of the test samples. The compounds were initially dissolved in neat DMF and an aliquot sample solution was diluted to twice the desired final maximum test concentration with serum-free medium. Four additional serial dilutions were performed to

provide a total of five sample concentrations. Aliquots of 100 μL of these different sample dilutions were added to the appropriate wells, which already contained 100 μL medium, resulting in the required final sample concentrations. Following addition of the samples, the plates were incubated for an additional 48 h at 37 °C, 5% CO_2, 95% air and 100% relative humidity. The medium without samples served as a control and triplicate measurements were made for all concentrations.

MTT assay

3-[4,5-Dimethylthiazol-2-yl]-2,5-diphenyltetrazolium bromide (MTT) is a yellow water-soluble tetrazolium salt. A mitochondrial enzyme in living cells, succinate dehydrogenase, cleaves the tetrazolium ring, converting MTT into an insoluble purple formazan. Therefore, the amount of formazan that is produced is directly proportional to the number of viable cells. After 48 h incubation, 15 μL MTT (5 mg mL^{-1}) in phosphate buffered saline (PBS) was added to each well and incubated at 37 °C for 4 h.

The quantity of formazan formed gave a measure of the number of viable cells. HeLa, MCF-7, and NIH 3T3 cells were used for the MTT assay. The absorbance was monitored at 570 nm (measurement) and 630 nm (reference) using a 96-well plate reader (Bio-Rad, Hercules, CA, USA). Data were collected for four replicate measurements each and used to calculate the respective means. The percentage inhibition was calculated from this data using the formula:

$$\%\ \text{cell inhibition} = 1 - \text{Abs (sample)/Abs (control)} \times 100$$

The IC_{50} value was calculated as the concentration of the complex that was required to reduce the absorbance to half that of the control.

Neutral red uptake assay

This test was performed according to well-known standard methods.[50] Cells were plated in 96-well plates (40 000 cells per well) and incubated in DMEM + 10% FBS for 24 hours at 37 °C and 5% CO_2. The complexes were then added at different concentrations for an additional 24 hours. The cells were then washed with PBS, after which 200 μL of a 0.625 μg mL^{-1} solution of neutral red was added. After 3 h, the cells were again washed with PBS to remove the remaining dye. The addition of 200 μL ethanol/acetic acid (50/1) resulted in release of the dye from the cells, which were placed in a shaking bath until a homogeneous colour was formed (approx. 1 h). The optical density was measured with a spectrometer at 540 nm.

Fluorescent double-staining experiment

Staining with acridine orange and ethidium bromide (AO and EB) was performed as follows: a cell suspension of each sample containing 5×10^5 cells was treated with 25 μL AO/EB solution (1 part 100 μg mL^{-1} of AO in PBS; 1 part of μg mL^{-1} of EB in PBS) and examined at 20× magnification under a LSM 710 laser scanning confocal microscope (Carl Zeiss, Germany) using a UV filter (450–490 nm). Three hundred cells per sample were counted in triplicate for each dose point. Cells were scored as viable, apoptotic or necrotic judging by the staining, nuclear morphology and membrane integrity. Morphological changes were also observed and photographed.

DAPI staining method

Staining with DAPI (4′,6-diamidino-2-phenylindole) was carried out using the following procedure: 5×10^5 cells were treated with the complex (100 μg mL^{-1}) for 24 h in a six-well culture plate and fixed with 4% paraformaldehyde followed by permeabilization with 0.1% Triton X-100. The cells were then stained with 50 μg mL^{-1} DAPI for 30 min at room temperature. The cells that were undergoing apoptosis, represented by morphological changes in apoptotic nuclei, were observed and imaged by ten views at 20× magnification under a LSM 710 laser scanning confocal microscope (Zeiss).

Apoptosis evaluation – flow cytometry

Cells were grown in six-well plates and exposed to three different concentrations of nickel(II) benzhydrazone complex 4 for 48 h. The annexin V-FITC kit uses annexin V conjugated to fluorescein isothiocyanate (FITC) to label phosphatidylserine sites on the membrane surface of apoptotic cells. In brief, the cells were trypsinised, washed with annexin-binding buffer, incubated with annexin V FITC and PI for 30 minutes and immediately analysed using a FACSAria-II flow cytometer. The results were analysed using DIVA software and the percentage of positive cells was calculated.

Results and discussion

Benzhydrazone ligand derivatives were prepared in high yield by the condensation of thiophene aldehydes with substituted benzhydrazides in an equimolar ratio. These ligands were allowed to react with $(CH_3COO)_2Ni \cdot 4H_2O$ in a 1 : 2 molar ratio in a DMF/ethanol medium under reflux for 5 h to afford new square-planar nickel(II) benzhydrazone complexes of the formula $[Ni(L)_2]$ (Scheme 1). In this reaction, the acetate anion acted as a base and promoted the formation of these complexes. The oxidation state of nickel remained unchanged during the formation of the complex. All the complexes were orange in colour, air-stable in both solid and liquid states at room temperature and non-hygroscopic. The synthesized nickel(II) benzhydrazone complexes were sparingly soluble in solvents such as chloroform, dichloromethane or acetonitrile and readily soluble only in solvents such as dimethylformamide (DMF) and dimethyl sulphoxide (DMSO), producing intensely orange-coloured solutions. The analytical data of all the nickel(II) benzhydrazone complexes are in good agreement with the proposed molecular structures.

The IR spectra of the free ligands displayed a medium to strong band in the region of 3254–3296 cm^{-1}, which is characteristic of the N–H functional group. The free ligands also displayed $\nu_{C=N}$ and $\nu_{C=O}$ absorptions in the region of 1636–1644 cm^{-1}, which indicate that the ligands exist in the amide

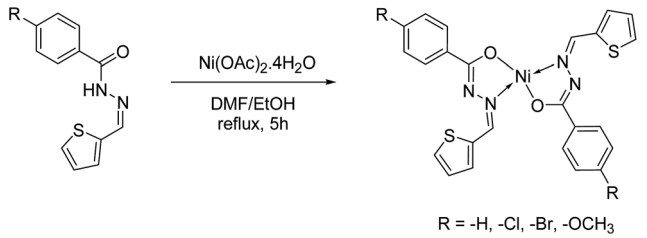

Scheme 1 Synthesis of nickel(II) benzhydrazone complexes.

form in the solid state. Bands that are due to ν_{N-H} and $\nu_{C=O}$ stretching vibrations were not observed with the complexes, which indicates that the ligands underwent tautomerization and subsequent coordination of the imidolate enolate form during complexation. Coordination of the ligand to the nickel(II) ion through an azomethine nitrogen is expected to reduce the electron density in the azomethine link and thus lower the absorption frequency after complexation (1520–1583 cm^{-1}), which indicates the coordination of azomethine nitrogen to the nickel(II) ion. The presence of a new band in the region of 440–470 cm^{-1}, which is due to $\nu_{(Ni-N)}$, is another indication of the involvement of the nitrogen of the azomethine group in coordination.[52] The band in the region of 1238–1250 cm^{-1} is due to the imidolate oxygen, which is coordinated to the metal.[53] The IR spectra of all the complexes therefore confirm the mode of coordination of the benzhydrazone ligand to the nickel(II) ion *via* the azomethine nitrogen and imidolate oxygen.

The absorption spectra of all the nickel(II) benzhydrazone complexes **1–4** were obtained in dimethylformamide solution in the range of 200–800 nm at room temperature and all the complexes exhibited three bands with absorption maxima in the region of 265–426 nm, as shown in Fig. S1–S4 (ESI†). The electronic spectrum of the hydrazone ligand in DMF solution displayed two broad absorption bands at 268 and 323 nm, which correspond to π–π* and n–π* transitions, respectively. The former band is due to π–π* transitions within the aromatic rings and remains almost unchanged in the spectra of the metal complexes, whereas the second band, which is due to n–π* transitions within the >C=N–N chromophore, is shifted to a longer wavelength as a consequence of coordination when binding to the metal atom, which confirms both the formation of the metal complexes and the fact that the azomethine nitrogen is involved in coordination.[54] The UV-vis spectra of the nickel(II) complexes exhibited bands in the region of 265–272 nm, which correspond to ligand-centered (LC) transitions. The other high-intensity band, which was observed in the region of 361–365 nm, is due to a nitrogen-metal charge transfer (LMCT) absorption band. The longer-wavelength band in the region of 421–426 nm corresponds to d–d transitions of d^8 low-spin Ni^{II} with slightly distorted square-planar geometry.

The ^1H NMR spectra of the complexes in DMSO gave very broad signals, which suggest that ligand exchange took place in the DMSO solution. However, we obtained mass spectra for all the complexes that confirm the formation of nickel(II) benzhydrazone complexes, as shown in Fig. S5–S8 (ESI†). Mass spectrometric measurements were carried out under positive/negative-ion ESI conditions with different cone voltages using DMF as the solvent and mobile phase. The ESI spectra of complexes **1** and **2** exhibit base peaks at *m*/*z* 522.85 and *m*/*z* 592.57, respectively, whereas complexes **3** and **4** display base peaks at *m*/*z* 682.70 and *m*/*z* 577.48, respectively.

Single-crystal X-ray crystallography

Attempts were made to grow single crystals for X-ray diffraction to confirm the molecular structures and geometry of all the synthesised complexes. However, we could not succeed in obtaining single crystals except for complex **4** [$Ni(L4)_2$], owing to solubility problems. The crystal structure of complex **4** is shown in Fig. 1 and relevant crystallographic data are listed in Table 1. The complex crystallizes in the $P2_1/c$ space group. The nickel ion is tetracoordinated in the square-planar geometry by two benzhydrazone ligand molecules that act as monoanionic bidentate N,O-donors *via* the azomethine nitrogen and deprotonated amide oxygen in the benzhydrazone fragment, forming two fused five-membered chelate rings. The ligands are in the *trans* position with respect to the C–N bonds and the complex is centrosymmetric around the nickel center. The nickel atom therefore sits in a N_2O_2 coordination environment, which is square-planar in nature as indicated by all the bond parameters around the nickel atom. In the complex, the benzhydrazone ligands bind to the metal center *via* N and O forming two five-membered chelate rings with bite angles N(1)–Ni(1)–O(1) of 96.1(1)° and O(1)–Ni(1)–N(1) of 83.9(1)°. The bond lengths of Ni(1)–N(1) and Ni(1)–O(1) are 1.850(2) and 1.838(2) Å, respectively. The bond lengths and bond angles as given in Table 2 are in good agreement with reported data on related nickel(II) complexes with square-planar geometry.[55] Because all four nickel(II) complexes exhibit similar spectral properties, the other three complexes are considered to have a similar structure to that of complex **4**. X-ray determination confirms the structure that was proposed on the basis of spectroscopic data, which is consistent with the bivalency of the metal and the monoionic nature of the ligand in the complexes.

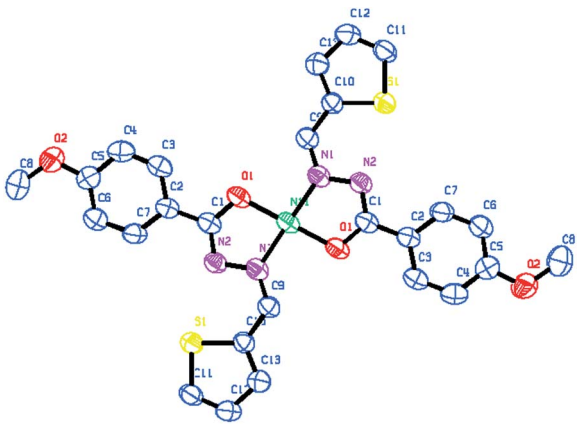

Fig. 1 Molecular structure of complex **4** (hydrogen atoms are omitted for clarity; displacement parameters are drawn at 50% probability level).

Electron-transfer properties

Electrochemical studies were carried out for all the free ligands and nickel(II) benzhydrazone complexes in DMF solution under an atmosphere of nitrogen in the potential range from +1.4 to −1.4 V. Tetrabutylammonium perchlorate (TBAP) (0.05 M) was used as the supporting electrolyte and the concentration of the complexes was $\sim 10^{-3}$ M. The potentials of all the nickel(II) benzhydrazone complexes are summarized in Table 3 and cyclic voltammograms of all the complexes are shown in Fig. S9–S12 (ESI†). We did not observe any redox waves within the potential limits from +1.4 to −1.4 V for free ligands and therefore all the responses that were observed within these potential limits were due to the metal centre only. All the complexes displayed a quasi-reversible reduction ($Ni^{II} \rightarrow Ni^{I}$) at a scan rate of 100 mV s^{-1}. The single-electron nature of the voltammograms was confirmed by a comparison of the current heights for the complexes and that for a simple $[Fe(bipy)_3]^{2+}$ complex under identical conditions.[56] All the complexes exhibited well-defined reduction waves with $E_{1/2}$ in the range from −0.71 to −0.77 V. The redox processes were quasi-reversible in nature and characterized by a rather large peak-to-peak separation (ΔE_p) of 210–310 mV.[57] The redox potentials were virtually independent of the scan rates, which indicates quasi-reversibility.[58] In general, the reason for quasi-reversible electron transfer in the above complexes may either be due to slow electron transfer or the deposition of the complex on the electrode surface.

The Ni^{II}/Ni^{I} reduction potential has been found to be sensitive to the nature of the substituent R in the thiophene aldehyde benzhydrazone ligand, which perturbs the reduction of the metal. The potential increases linearly with an increase in the electron-withdrawing character of R. A plot of formal potential $E_{1/2}$ *versus* σ (where σ is the Hammett substituent constant[59] of R; σ values for R: $OCH_3 = -0.27$, H = 0.00, Cl = +0.23, Br = +0.23) is found to be linear for the reduction couples, as shown in Fig. 2. The slope of this line, which is known as the reaction constant, ρ, is a measure of the sensitivity of $E_{1/2}$ to the substituent (R) for the Ni^{II}/Ni^{I} couple. This shows that the nature of the *para*-substituent R on the thiophene aldehyde benzhydrazone ligands can influence the potentials of metal centers in a predictable manner.

Table 2 Selected bond lengths (Å) and bond angles (°) for complex **4**

Complex	**4**
Ni(1)–O(1)	1.838(2)
Ni(1)–N(1)	1.850(2)
O(1)–C(1)	1.306(3)
O(2)–C(5)	1.358(3)
O(1)–C(8)	1.420(5)
S(1)–C(10)	1.724(2)
S(2)–C(11)	1.703(4)
N(1)–N(2)	1.379(3)
N(1)–C(9)	1.300(4)
N(2)–C(1)	1.317(4)
O(1)–Ni(1)–O(1)	180.0(9)
N(1)–Ni(1)–N(1)	180.0(1)
O(1)–Ni(1)–N(1)	83.9(1)
N(1)–Ni(1)–O(1)	96.1(1)
N(1)–N(2)–C(1)	108.2(2)
S(1)–C(10)–C(13)	110.8(2)
Ni(1)–O(1)–C(1)	110.9(2)
Ni(1)–N(1)–N(2)	114.4(2)
N(1)–C(9)–H(9)	116.3(3)
N(2)–N(1)–C(9)	116.6(2)
N(2)–C(1)–C(2)	119.1(3)
O(1)–C(1)–N(2)	122.6(3)
S(1)–C(10)–C(9)	125.6(2)
Ni(1)–N(1)–C(9)	129.1(2)

Table 3 Cyclic voltammetry data of the nickel(II) benzhydrazone complexes[a]

Complexes	E_{pc} (V)	E_{pa} (V)	$E_{1/2}$ (V)	ΔE_p (mV)
1	−0.87	−0.58	−0.73	290
2	−0.88	−0.67	−0.77	210
3	−0.89	−0.62	−0.76	270
4	−0.87	−0.56	−0.71	310

[a] Solvent = dimethylformamide; [complex] = 1×10^{-3} M; supporting electrolyte: $[Bu_4N](ClO_4)$ (0.05 M); scan rate: 100 mV s^{-1}; E_{pa} and E_{pc} = anodic and cathodic peak potentials, respectively; $E_{1/2} = 0.5(E_{pc} + E_{pa})$; $\Delta E_p = (E_{pc} - E_{pa})$; all potentials are referenced to SCE.

DNA-binding studies

DNA is the primary pharmacological target of many antitumor compounds. DNA–metal complex interactions are of paramount importance in understanding the mechanism of tumour inhibition in the treatment of cancer. The interaction of nickel(II) benzhydrazone complexes **1–4** with CT-DNA was studied by a number of techniques such as absorption spectral titration, fluorescence spectroscopy, cyclic voltammetry, circular dichroism and viscosity measurements.

UV-vis absorption studies

Electronic absorption spectroscopy is commonly employed to determine the binding ability of metal complexes with a DNA helix. Complexes that bind to DNA by intercalation are characterised by a change in absorbance (hypochromism) and

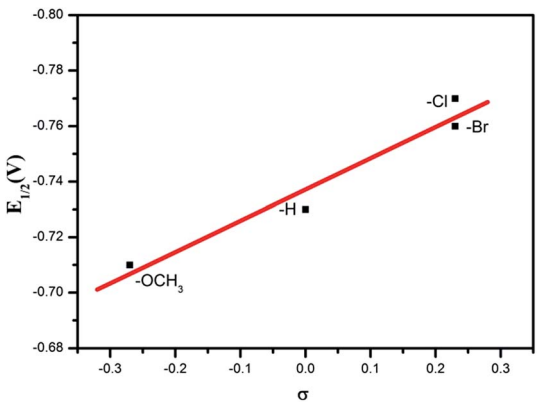

Fig. 2 Least-squares plot of $E_{1/2}$ values for the Ni^{II}/Ni^{I} reduction potential *vs.* σ.

bathochromic shift in wavelength, which are due to a strong stacking interaction between the aromatic chromophore of the test complex and DNA base pairs.[60] The extent of hypochromism is commonly related to the strength of intercalation.[61] The interaction of the complexes with CT-DNA was monitored by obtaining the UV-visible spectra of the system. The experiment was carried out by keeping the concentration of the nickel(II) benzhydrazone complexes (25 μM) constant and changing the concentration of CT-DNA (0–60 μM). The absorption bands at 273 nm and 321 nm for the complexes were studied for corresponding changes in absorptivity upon the incremental addition of CT-DNA.

The absorption spectra of complexes **1–4** in the absence and presence of CT-DNA are shown in Fig. 3. From the electronic absorption spectral data, it is clear that with an increase in the concentration of DNA added to the nickel(II) complexes **1–4** all the abovementioned absorption bands exhibited hypochromism of 34.14%, 34.82%, 34.05% and 41.92%, respectively, accompanied by bathochromic shifts of 2–3 nm, which shows that the nickel(II) benzhydrazone complexes were bound strongly to CT-DNA *via* the intercalative mode. The observed hypochromism was due to stacking interactions between the aromatic chromophores of the complexes and DNA base pairs, which is consistent with the intercalative mode of binding. These observations are similar to those that were reported earlier for various metallointercalators.[62] To compare the binding strengths of the complexes with CT-DNA, the intrinsic binding constant K_b was determined from eqn (1):

$$[DNA]/[\varepsilon_a - \varepsilon_f] = [DNA]/[\varepsilon_b - \varepsilon_f] + 1/K_b[\varepsilon_b - \varepsilon_f] \quad (1)$$

where [DNA] is the concentration of DNA in base pairs, ε_a is the extinction coefficient of the complex at a given DNA concentration, ε_f is the extinction coefficient of the complex in free solution and ε_b is the extinction coefficient of the complex when fully bound to DNA. A plot of $[DNA]/[\varepsilon_b - \varepsilon_f]$ *versus* [DNA] gave a slope and intercept that were equal to $1/[\varepsilon_b - \varepsilon_f]$ and $(1/K_b)$ $[\varepsilon_b - \varepsilon_f]$, respectively. K_b was calculated from the ratio of the slope to the intercept.

Values of the intrinsic binding constant (K_b) were calculated using the abovementioned equation and found to be $1.60(\pm0.10) \times 10^5$ M^{-1}, $2.84(\pm0.06) \times 10^5$ M^{-1}, $2.34(\pm0.08) \times 10^5$ M^{-1} and $3.55(\pm0.02) \times 10^5$ M^{-1}, corresponding to complexes **1–4**. From this experimental result, it is very clearly shown that an increase in the electron-donating ability of the substituent present in the ligand increases the DNA-binding ability of the complex. The presence of electron-withdrawing groups in complexes **2** and **3** results in almost comparable values of the binding constant. Complex **1** has a lower binding constant, which may be due to the presence of H as a substituent. Electronic absorption titration studies reveal that all the complexes interact with DNA *via* the intercalative mode and complex **4** binds to CT-DNA more strongly than the other complexes. The binding mode needs to be proved by further experiments.

Emission quenching titration

EB is a general fluorescent probe for DNA structures and has been used in examinations of the mode and process of the binding of metal complexes to DNA. The fluorescence emissions of EB bound to DNA in the presence of nickel(II) benzhydrazone complexes are shown in Fig. 4. The intensity of the emissions of the EB–DNA system (λ = 595 nm) apparently decreased as the concentration of the complexes increased, which indicates that the complexes replaced EB in the DNA–EB system. The resulting decrease in fluorescence was caused by EB moving from a hydrophobic environment to an aqueous environment.

The quenching constant was calculated from the Stern–Volmer eqn (2):

$$I_0/I = 1 + K_q[Q] \quad (2)$$

where I_0 is the emission intensity in the absence of the quencher, I is the emission intensity in the presence of the quencher, K_q is

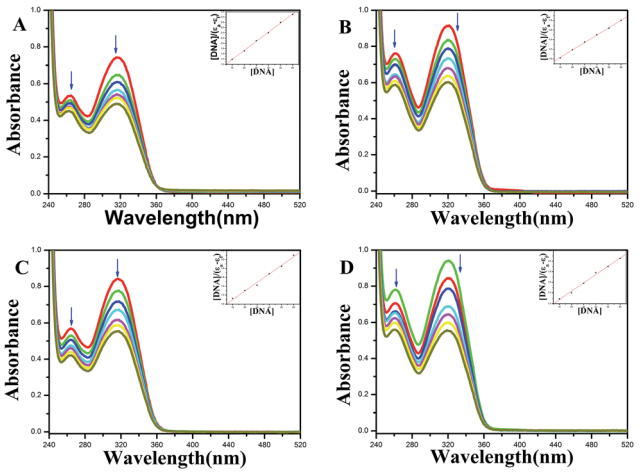

Fig. 3 Electronic absorption spectra of complexes bound to DNA: **1** (A), **2** (B), **3** (C) and **4** (D). [DNA] = 0–60 μM, [complex] = 25 μM (inset: plot of $[DNA]/(\varepsilon_a - \varepsilon_b)$ *vs.* [DNA]).

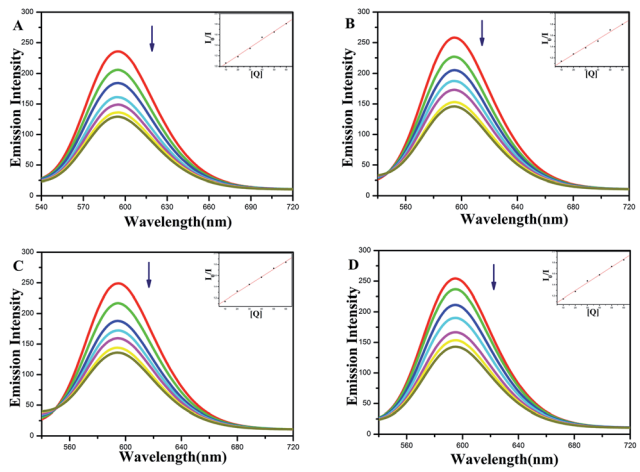

Fig. 4 Fluorescence quenching curves of EtBr bound to DNA: **1** (A), **2** (B), **3** (C) and **4** (D). [DNA] = 10 μM, [EB] = 10 μM, [complex] = 0–60 μM (inset: plot of I_0/I *vs.* [Q]).

the quenching constant, and [Q] is the quencher concentration. K_q is the slope that is obtained from a plot of I_0/I *versus* [Q] (shown as insets in Fig. 4). The quenching plots illustrate that the quenching of EtBr bound to CT-DNA by the nickel(II) benzhydrazone complexes is in good agreement with the linear Stern–Volmer equation. The K_q values that were obtained from the experiments are $1.01(\pm0.14) \times 10^5$ M^{-1}, $1.03(\pm0.10) \times 10^5$ M^{-1}, $1.03(\pm0.12) \times 10^5$ M^{-1} and $1.04(\pm0.08) \times 10^5$ M^{-1}, respectively. Furthermore, the apparent DNA-binding constant (K_{app}) was calculated from the following eqn (3):

$$K_{EtBr}[EtBr] = K_{app}[complex] \quad (3)$$

where the concentration of the complex has the value that corresponds to a 50% reduction in the fluorescence intensity of EtBr, $K_{EtBr} = 1.0 \times 10^7$ M^{-1} and [EtBr] = 10 μM, and was found to be 5.26×10^5 M^{-1}, 5.35×10^5 M^{-1}, 5.81×10^5 M^{-1}, and 6.25×10^5 M^{-1} for complexes **1–4**, respectively.

The fluorescence quenching spectra of DNA-bound EtBr in the presence of complexes **1–4** shown in Fig. 4 illustrate that as the concentration of the complexes increased, the emission band at 595 nm (545 nm excitation) exhibited hypochromism of up to 44.85%, 44.53%, 45.73% and 46.20% with a hypsochromic shift of 2–3 nm in the initial fluorescence intensity for complexes **1–4**, respectively. The observed decrease in fluorescence intensity clearly reveals that EtBr molecules were displaced from their DNA binding sites by the complexes under investigation.[63]

Cyclic voltammetry

The different modes of interaction of metal complexes with DNA can be studied not only by electronic absorption spectral studies but also by cyclic voltammetry. In order to investigate the mode of interaction between the nickel(II) hydrazone complexes and DNA, a cyclic voltammetry experiment was carried out. In general, the electrochemical potential of a small molecule will shift in a positive direction when it intercalates into a DNA double helix and in a negative direction in the case of electrostatic interaction with DNA.[64,65]

In CV titration, both the concentration and volume of the analyte were kept constant while changing the concentration of DNA in the solution. The typical CV behaviour of the nickel(II) hydrazone complexes [Ni(L1)$_2$] in the absence and presence of different concentrations of CT-DNA is shown in Fig. 5. When CT-DNA was added to a solution of a complex, both anodic and cathodic peak current heights of the complex decreased in the same manner during the addition of increasing amounts of DNA. Furthermore, during the addition of DNA, the anodic peak potential (E_{pa}), cathodic peak potential (E_{pc}) and $E_{1/2}$ (calculated as the average of E_{pc} and E_{pa}) all exhibited positive shifts. These positive shifts are considered as evidence of the intercalation of the complex into DNA, because this type of interaction is due to hydrophobic interaction. From another point of view, if a molecule binds electrostatically to the negatively charged deoxyribose phosphate backbone of DNA, a negative peak potential should be detected. Therefore, the positive shift in the CV peak potential

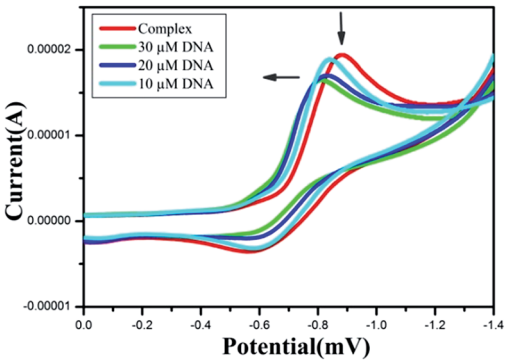

Fig. 5 Cyclic voltammetry measurements at a scan rate of 100 mV s^{-1}. [Complex] = 10 μM and [CT-DNA] addition (0–30 μM).

of the nickel(II) hydrazone complexes is indicative of an intercalative binding mode with DNA molecules.[66]

Circular dichroism spectral study

CD has been effectively used to interpret the conformational changes of DNA upon binding to a metal complex. The circular dichroism spectrum of DNA displays a positive band at 275 nm (UV-vis: λ_{max} 258 nm), which is due to base stacking, and a negative band at 245 nm, which is due to the helicity of B-type DNA.[67] Simple groove binding and electrostatic interaction of the molecules give rise to little or no perturbation in base stacking and helicity, although intercalation increases the intensities of both the positive and negative bands. The CD spectrum of CT-DNA (60 μM) in the presence of complex **1** (20 μM) is shown in Fig. 6. From the experimental results, we observed that the addition of the complexes to the DNA system increased the intensity of both the positive and negative bands of free DNA, which is clear evidence of intercalation between the nickel(II) benzhydrazone complexes and CT-DNA. The CD spectra indicate that the binding of complexes **1–4** to CT-DNA results in significant increases in the intensities of both positive and negative bands without any shift in peak positions, which shows that the binding of complexes does not lead to any significant change in the conformation of CT-DNA.[61]

Viscosity studies

To further investigate the binding of the nickel(II) benzhydrazone complexes, viscosity measurements were carried out on calf thymus DNA by varying the concentration of the added complex. Optical photophysical probes generally provide clues that are necessary, but not sufficient to support a binding model. Viscosity measurements that are sensitive to changes in length are regarded as the least ambiguous and most critical tests of binding model in a solution in the absence of crystallographic structural data or NMR.[68] A classical intercalation model results in a lengthening of the DNA helix, as base pairs are separated to accommodate the binding ligand, which leads to an increase in the viscosity of DNA. However, partial and/or non-classical intercalation of a ligand may bend or kink the

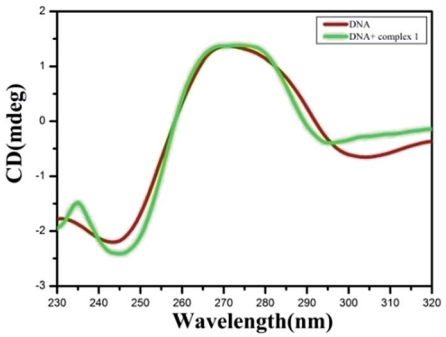

Fig. 6 Circular dichroism spectrum of CT-DNA (60 μM) in the presence of complex **1** (20 μM).

DNA helix, resulting in a decrease in its effective length and consequently its viscosity.[69]

The effects of the nickel(II) complexes on the viscosity of CT-DNA are shown in Fig. 7. Values of $(\eta - \eta_o)^{1/3}$, where η and η_o are the specific viscosities of DNA in the presence and absence of the complexes, are plotted against [complex]/[DNA]. The relative viscosity of CT-DNA exhibits a considerable increase in the presence of increasing amounts of the complexes. Such behaviour indicates that the complexes are inserted between the DNA bases, thus resulting in an intercalative mode of binding between DNA and each complex. The ability of the complexes to increase the viscosity of DNA follows the order **1** < **3** < **2** < **4**.

Protein-binding studies

Fluorescence quenching of BSA by nickel(II) benzhydrazone complexes. It is well known that the transport of drugs through the bloodstream is affected by the interaction of drugs with blood plasma proteins, in particular serum albumin. Analysis of the binding of chemical compounds to BSA is commonly undertaken by examining fluorescence spectra. The binding of BSA to the nickel(II) benzhydrazone complexes was studied by fluorescence measurements at room temperature. Various concentrations of complexes **1–4** were added to solutions of BSA (1 μM) and fluorescence spectra were obtained in the range of 300–450 nm upon excitation at 280 nm. The effects of the complexes on the fluorescence emission spectrum of BSA are given in Fig. 8. Upon addition of the nickel(II) benzhydrazone complexes to a solution of BSA at an emission wavelength of 345 nm, decreases of up to 40.12%, 35.84%, 34.64% and 43.06% from the initial fluorescence intensity of BSA accompanied by a hypsochromic shift of 3–5 nm for complexes **1–4**, were observed, respectively.

The blue shift that was observed was mainly due to the fact that the active site of the protein is buried in a hydrophobic environment. These results suggest a strong interaction of all the complexes with the BSA protein. Fluorescence quenching is described by the Stern–Volmer relation:

$$I_0/I = 1 + K_{sv}[Q] \quad (4)$$

where I_0 is the emission intensity in the absence of the quencher, I is the emission intensity in the presence of the quencher, K_{sv} is the Stern–Volmer quenching constant, and [Q] is the quencher concentration. K_{sv} is the slope that is obtained from a plot of I_0/I *versus* [Q] (shown in Fig. 9A) and was found to be $1.02(\pm0.04) \times 10^6$ M^{-1}, $1.01(\pm0.07) \times 10^6$ M^{-1}, $1.01(\pm0.18) \times 10^5$ M^{-1} and $1.02(\pm0.15) \times 10^6$ M^{-1}, corresponding to complexes **1–4**. It is assumed that the binding of compounds to BSA occurs with an equilibrium binding constant and can be analysed according to the Scatchard equation:

$$\log[(F_O - F)/F] = \log K + n \log[Q] \quad (5)$$

where K and n are the binding constant and number of binding sites, respectively. A plot of $\log[(F_O - F)/F]$ *versus* log[Q] can be used to determine the values of both K and n and values that were calculated for complexes **1–4** from Fig. 9 are listed in Table 4. From the values of n, it is clearly shown that there is only one independent class of binding sites for the complexes on BSA and also a direct relation between the binding constant and the number of binding sites.

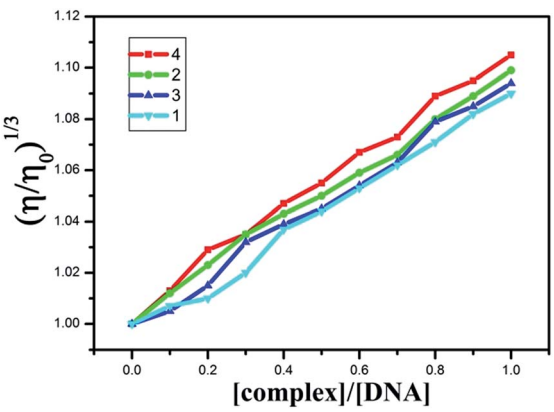

Fig. 7 Effect of increasing amounts of complexes **1–4** on the relative viscosity of CT-DNA at 29.0 ± 0.1 °C. [DNA] = 5 μM and [complexes] = 0–5 μM.

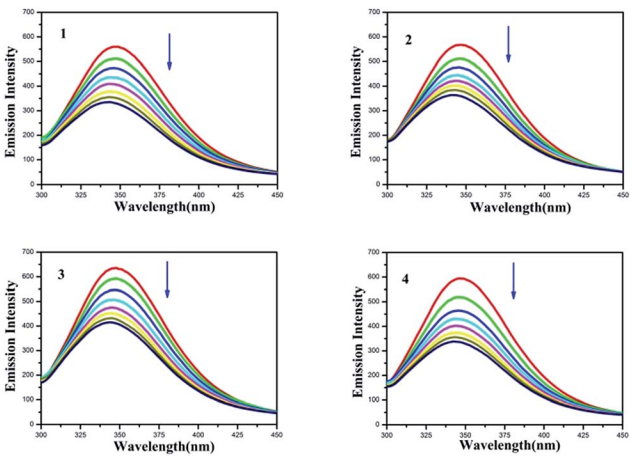

Fig. 8 Emission spectra of BSA at various concentrations of complexes **1–4**. [BSA] = 1 μM and [complexes] = 0–70 μM.

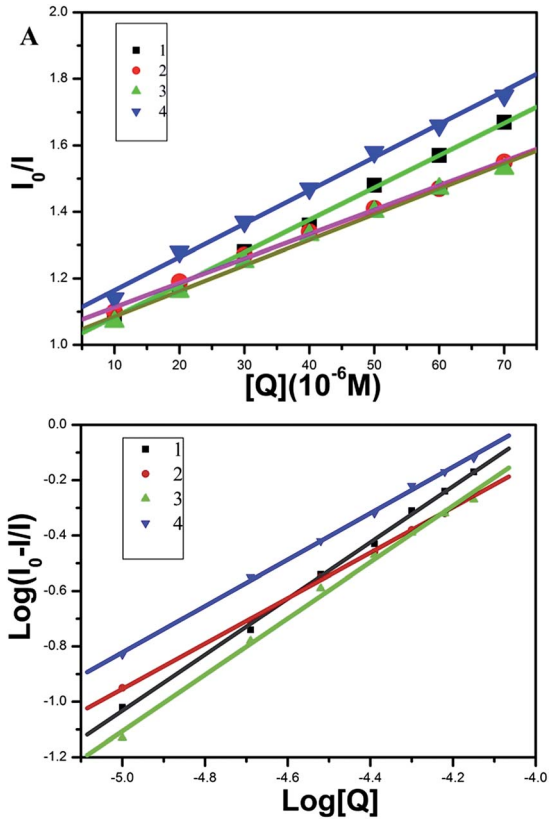

Fig. 9 Stern–Volmer plots (A) and Scatchard plots (B) of the fluorescence titration of complexes **1–4** with BSA.

Larger values of K_{bin} and K_q reveal that strong interaction occurs between BSA and the complexes. The calculated value of n is around 1 for all the complexes, which indicates the existence of a single binding site in BSA for all the complexes. The results of the binding constant values indicate that the complexes bind to BSA in the order of **4** > **2** > **3** > **1**. Complex **4** can interact with the active site by making it more hydrophobic. Among the four nickel(II) benzhydrazone complexes, complex **4** exhibits a stronger interaction with BSA than the other nickel(II) benzhydrazone complexes.

UV-vis absorption studies

Commonly, quenching occurs *via* either static or dynamic quenching. Dynamic quenching is a process in which a fluorophore and a quencher come into contact during the transient existence of an excited state, whereas static quenching refers to the formation of a fluorophore–quencher complex in the ground state. A simple method to determine the type of quenching is UV-visible spectroscopy. Fig. 10 shows the UV-vis spectra of BSA in the presence and absence of the complexes, which indicates that the absorption intensity of BSA increased as the complexes were added and there was a small blue shift of about 2 nm for all the complexes. This revealed the existence of a static interaction between BSA and the complexes.[60]

Table 4 Binding constants and number of binding sites for the interactions of nickel(II) benzhydrazone complexes **1–4** with BSA

System	K (M^{-1})	n
BSA + complex **1**	$1.07(\pm0.08) \times 10^6$	$1.01(\pm0.01)$
BSA + complex **2**	$1.51(\pm0.04) \times 10^6$	$0.82(\pm0.05)$
BSA + complex **3**	$1.08(\pm0.23) \times 10^6$	$1.02(\pm0.15)$
BSA + complex **4**	$2.40(\pm0.06) \times 10^6$	$0.84(\pm0.10)$

Characteristics of synchronous fluorescence spectra

Synchronous fluorescence spectra provide information on the molecular environment, in particular in the vicinity of the functional groups of a fluorophore.[70] It is well known that the fluorescence of a protein may be due to the presence of tyrosine, tryptophan and phenylalanine residues and therefore spectroscopic methods are usually applied to investigate conformational changes of a serum protein. According to Miller,[71] in synchronous fluorescence spectroscopy, the difference between the excitation and emission wavelengths ($\Delta\lambda = \lambda_{emi} - \lambda_{exc}$) is indicative of the spectra of different types of chromophores; a small $\Delta\lambda$ value such as 15 nm is characteristic of tyrosine residues and a large $\Delta\lambda$ value such as 60 nm is characteristic of tryptophan residues. In order to study the structural changes of BSA in the presence of nickel(II) hydrazone complexes, we obtained synchronous fluorescence spectra on the addition of complexes **1–4**.

The synchronous fluorescence spectra of BSA with nickel(II) hydrazone complexes **1–4** were obtained at both $\Delta\lambda = 15$ nm and $\Delta\lambda = 60$ nm and are shown in Fig. 11 and 12. In the synchronous fluorescence spectra of BSA at $\Delta\lambda = 15$ nm, increasing the concentration of the complexes in the solution of BSA resulted in decreases in the fluorescence intensity of BSA at 302 nm of 30.84%, 32.78%, 33.18% and 34.71% of the initial fluorescence intensity of BSA and a red shift of 1–2 nm for complexes **1–4**, respectively. However, in the case of the synchronous fluorescence spectra of BSA at $\Delta\lambda = 60$ nm, an increase in the concentration of the complexes in the solution of BSA resulted in significant decreases in the fluorescence intensity at 345 nm of up to 51.40%, 37.71%, 34.20% and 51.75% of the initial fluorescence intensity of BSA accompanied by a blue shift of 1–2 nm for complexes **1–4**.

These experimental results indicate that nickel(II) benzhydrazone complexes do not affect the conformation with residues led to a decrease in the polarity of the fluorophore by

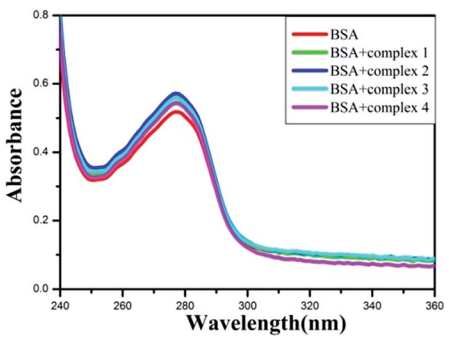

Fig. 10 Absorption spectra of BSA (1×10^{-5} M) in the presence of complexes **1–4** (5 μM).

increasing the hydrophobicity in its environment. Hence, the strong interaction between the complexes and BSA demonstrates that these complexes can easily be stored in the protein and can be released at desired targets. The characteristics of the synchronous fluorescence measurements show that conformational changes occurred in BSA upon interaction with nickel(II) benzhydrazone complexes.

BSA cleavage studies

The ability of the complexes to cleave protein peptide bonds[72] was studied using BSA as a substrate. The experiment was carried out using BSA (20 μM) in 5 mM Tris–HCl-50 mM NaCl buffer at pH = 7.2. In the absence of an activator such as hydrogen peroxide, none of the complexes give rise to any protein cleavage even at a concentration of 500 μM. When the cleavage experiment was performed at a concentration of the complex of 200 μM in the presence of H_2O_2 (100 μM) at pH 7.2 (Fig. 13), all the complexes produce significant smearing or fading of the BSA band, which suggests that the complexes bind non-specifically to the protein and cleave BSA into very small fragments. All the complexes are capable of cleaving the protein but without any sequence specificity.

Antioxidant activity

In order to determine the ability of the nickel(II) benzhydrazone complexes to act toward different reactive species, we studied some radical-scavenging assay methods, in particular DPPH, OH and NO radical-scavenging assays (Fig. 14). The hydrazone ligands, metallic precursors and nickel(II) benzhydrazone complexes were tested in the range of 10–50 μM. It is to be noted that no significant radical-scavenging activity was observed for the ligands and metallic precursors under identical experimental conditions. From the experimental results, the IC_{50} values of the complexes with respect to the DPPH, OH and NO radical assays were found to be 41.6, 40, 40.8, and 34.5 μM, 41.6, 40.81, 40, and 35.0 μM, and 44.1, 43, 41.8 and 38.1 μM, respectively. The IC_{50} values show that the complexes exhibit

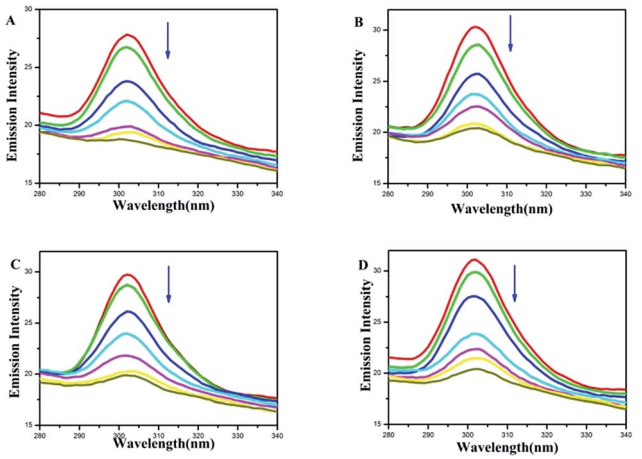

Fig. 11 Synchronous fluorescence spectra of BSA (1 μM) as a function of the concentration of complexes **1** (A), **2** (B), **3** (C), and **4** (D) (0–60 μM) with a difference in wavelength of $\Delta\lambda = 15$ nm.

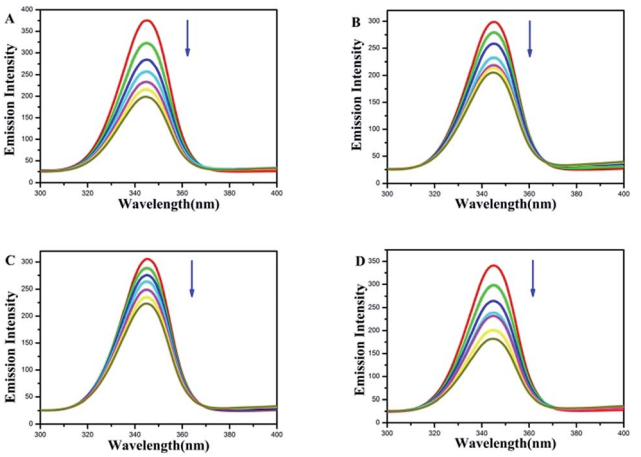

Fig. 12 Synchronous fluorescence spectra of BSA (1 μM) as a function of the concentration of complexes **1** (A), **2** (B), **3** (C), and **4** (D) (0–60 μM) with a difference in wavelength of $\Delta\lambda = 60$ nm.

antioxidant activity in the order of **4** > **2** > **3** > **1** ligand > precursors in all the experiments. Complexes **1–4** displayed almost comparable free-radical-scavenging activity with respect to the standard antioxidant (BHA). From the IC_{50} values, it can be concluded that the nickel complexes possess higher antioxidant activity when compared with the free ligands and metallic precursors, which is due to their chelation with metal ions. Among the complexes, complex **4** exhibits good radical-scavenging activity, which might be due to the greater electron-donating nature of the methoxy substituent and the planarity of the phenyl group. The lowest activity was observed for complex **1**. Hence, we strongly consider that the present metal hydrazone complexes can be further evaluated as suitable candidates leading to the development of new potential antioxidants and therapeutic reagents for some diseases.

Cytotoxicity

Preliminary up-to-date results are remarkably positive, supporting our facts and confirming the significant potential of

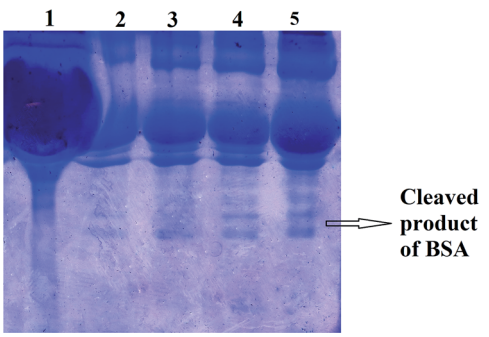

Fig. 13 SDS-PAGE diagram of the cleavage of bovine serum albumin (BSA) by complexes **1–4**. [BSA] = 20 μM, [complexes] = 200 μM in 5 mM Tris–HCl-50 mM NaCl buffer at pH = 7.2 and in the presence of hydrogen peroxide (H_2O_2, 100 μM) at 50 °C with an incubation time of 3 h. Lane 1 (control), BSA + H_2O_2; lane 2, BSA + H_2O_2 + **1**; lane 3, BSA + H_2O_2 + **2**; lane 4, BSA + H_2O_2 + **3**; lane 5, BSA + H_2O_2 + **4**.

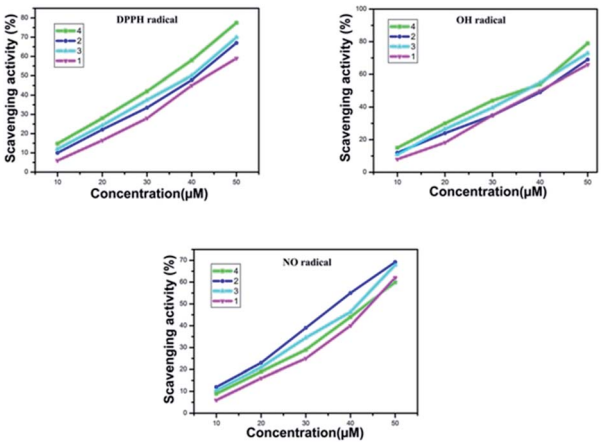

Fig. 14 Trends in the inhibition of DPPH, OH and NO radicals by complexes at various concentrations.

this class of nickel complexes as anticancer agents.[73] Nickel hydrazone complexes **1–4** were evaluated for their cytotoxicity against HeLa, MCF-7 and NIH-3T3 cell lines using a MTT assay after 48 hours of inhibition. For comparison, the cytotoxicity of the well-known anticancer drug cisplatin against all the abovementioned cell lines is shown in Table 5. The results were studied by means of cell viability curves and expressed as values in the studied concentration range from 0.1 to 100 μM. The activities that correspond to inhibition of cancer cell growth at a maximum level, expressed as IC_{50} values, which relate to inhibition of cancer cell growth at the 50% level, are noted.

It is to be noted that the precursor and ligand did not display any inhibition of cell growth, even at concentrations of up to 100 μM, which clearly indicates that chelation of the ligand with the metal ion is responsible for the observed cytotoxic properties of the complexes. The results of MTT assays revealed that the complexes exhibited notable activity against both HeLa and MCF-7 cell lines with respect to IC_{50} values, as represented in Table 5. The cytotoxic activity of complex **4** was found to be superior when compared with other complexes. The observed higher efficiency of complex **4** is related to the nature of the substitution of the benzhydrazone ligand that is coordinated to the nickel ion. Higher cytotoxicity is observed for complex **4**, which contains an electron-donating methoxy group that consequently increases the lipophilic character of the metal complex, which favours its permeation through the lipid layer of a cell membrane. Between the two different cell lines that were used in the study, the proliferation of the MCF-7 cell line was arrested to a greater extent than that of HeLa cells by the complexes. Although the abovementioned complexes were active against the cell lines in *in vitro* cytotoxicity experiments, none of the complexes could attain the effectiveness shown by the standard drug cisplatin (IC_{50} values 16.20 and 13.86 μM, respectively). The *in vitro* cytotoxic activity test also shows that the IC_{50} value of the complex against NIH-3T3 (non-cancerous cells) was found to be above 235 μM, which confirms that the complex is very specific for cancer cells compared with cisplatin. The IC_{50} values are much higher than those previously reported for other nickel complexes.[74]

Neutral red uptake assay

The IC_{50} values that were obtained from the MTT assay were further evaluated by a neutral red uptake assay using HeLa cell lines. The neutral red uptake assay provides a quantitative estimation of the number of viable cells in a culture. It is based on the ability of viable cells to incorporate and bind the supravital dye neutral red in their lysosomes. Dying cells have an altered membrane potential and therefore can no longer take up neutral red. The dye is applied to cells in different concentrations to allow the determination of the IC_{50} concentration (50% reduction of uptake) by measuring OD_{540}.

HeLa cells were exposed to different concentrations of the nickel(II) benzhydrazone complexes **1–4** for 48 h of incubation. The results show IC_{50} values of 50.0 ± 1.2, 33.2 ± 1.0, 36.5 ± 0.9 and 20.1 ± 1.0 μM for complexes **1–4**, respectively, and these values were found to be very close to those obtained from the MTT assay.

Morphological changes in AO/EB double staining by confocal study

Upon exposure to cytotoxic agents, cell death may take place *via* several modes; among these, apoptosis and necrosis are very common. Apoptosis or programmed cell death is characterized by cell shrinkage, blebbing of the plasma membrane, and chromatin condensation. To investigate morphological changes, the acridine orange/ethidium bromide (AO/EB) double-staining technique is frequently used. In order to investigate the mechanistic aspects of cell death and to determine changes in nuclear morphology, AO/EB double staining of MCF-7 cell lines that were treated with complex **4** (10 μM) was carried out and is shown in Fig. 15. The experiment was based on the discrimination of live cells from dead cells on the basis of morphological changes. Acridine orange passes through the plasma membrane and stains the DNA of live cells with the appearance of green fluorescence. On the other hand, EB is excluded from cells that have an intact plasma membrane and stains the DNA of dead cells, producing orange fluorescence. Cells that were incubated with complex **4** for 24 h and irradiated with visible light exhibited a significant reddish-orange emission, which is characteristic of apoptotic cells. The controls,

Table 5 Cytotoxic activity of the complexes, IC_{50} (μM)[a]

Complex	HeLa	MCF-7	NIH-3T3
1	52.3 ± 1.5	22.4 ± 2.1	235.60 ± 0.5
2	32.1 ± 1.8	18.2 ± 1.1	238.72 ± 1.4
3	37.1 ± 2.1	17.8 ± 1.9	242.32 ± 2.0
4	18.1 ± 1.9	16.3 ± 0.9	245.64 ± 1.1
Cisplatin	16.20 ± 0.70	13.86 ± 0.5	240.52 ± 0.6

[a] IC_{50} = concentration of the drug that is required to inhibit the growth of 50% of the cancer cells (μM).

which were incubated in the dark, displayed only a predominant green emission. Hence, the observed morphological changes reveal that complex **4** is able to induce cell death only *via* apoptosis.

Nuclear DAPI staining experiment by confocal study

To further confirm the mode of apoptosis, DAPI staining was also carried out. DAPI is a fluorescent nuclear stain that is excited by ultraviolet light and exhibits strong blue fluorescence when bound to DNA. Control cells and cells treated with complex **4** (100 μg mL^{-1}) were stained with DAPI and observed under a confocal microscope (Fig. 16). The control cells, which were permeabilized with detergent (0.1% Triton X-100), exhibited light, evenly stained contours of the nuclei, in contrast to the treated cells, which displayed typical characteristics of cells undergoing apoptosis. The treated cells were seen to possess fragmented or highly condensed nuclei, whereas bright-field images provide evidence of cell shrinkage and membrane blebbing, which were attributed to typical features of apoptotic cells. Necrotic nuclei were not observed with DAPI staining. Hence, DAPI staining indicates an apoptotic mode of cell death with the complex.

Evaluation of apoptosis-flow cytometry

The ability of nickel(II) benzhydrazone complexes to induce apoptosis was further investigated with the aid of flow cytometry, using the annexin V-FITC apoptosis detection kit to perform double staining with propidium iodide and annexin V-FITC.[51] Annexin V, which is a Ca^{2+}-dependent phospholipid-binding protein with a high affinity for the membrane phospholipid phosphatidylserine (PS), is quite helpful for identifying apoptotic cells with exposed PS. Propidium iodide is a standard flow cytometry viability probe used to distinguish viable from non-viable cells. MCF-7 cells were treated with complex **4** at three different concentrations for 48 h: see Fig. 17. The annexin V^+/PI^+ (Q_2) population represents cells undergoing apoptosis, which increased from 30.7% and 48.6% to 52.7% for 50 μM, 100 μM and 200 μM concentrations of the complexes. This observation is in good agreement with the results obtained from fluorescence staining methods.

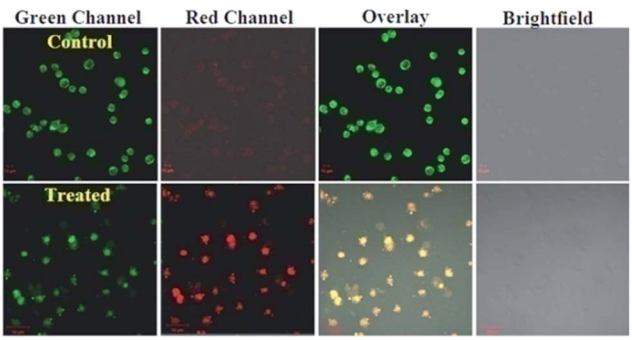

Fig. 15 AO/EB double staining of MCF-7 cells treated with complex **4** (10 μM) showing changes in nuclear morphology at 488–600 nm. The scale bar corresponds to 50 μm.

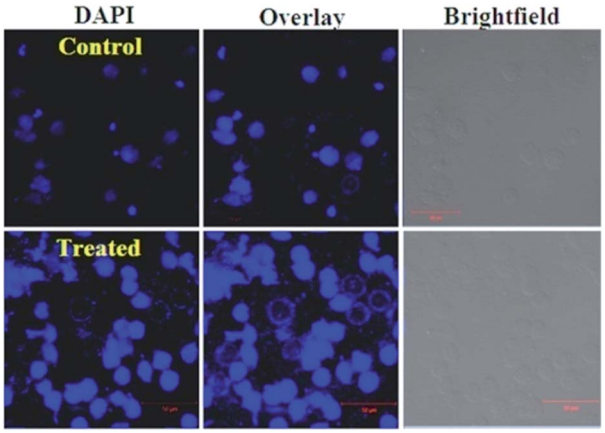

Fig. 16 Morphological assessment of complex **4** and MCF-7 cells for 24 h. Nuclei were stained with DAPI and observed under a confocal microscope at 458 nm.

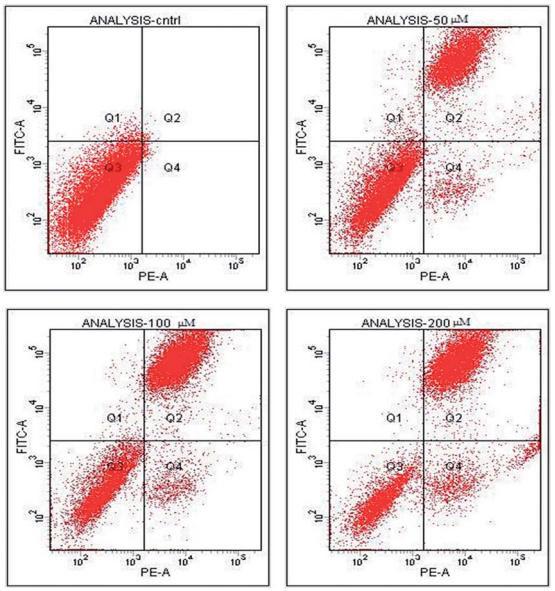

Fig. 17 Apoptosis assays: propidium iodide and annexin-positive (Q2) and propidium iodide-positive (Q4); flow cytometry results of untreated MCF-7 control cells and cells treated with complex **4** at 50 μM, 100 μM and 200 μM concentrations for 48 h, respectively.

Conclusion

The present study focuses on the synthesis and characterization of four new square-planar nickel(II) complexes with thiophene aldehyde benzhydrazone ligands. The characterization of the complexes was accomplished by analytical and spectral methods. All the complexes were found to have a metal : ligand molar ratio of 1 : 2. All the complexes exhibit a quasi-reversible one-electron reduction response *versus* SCE. The DNA-binding interactions of the complexes with CT-DNA show that the binding mode is essentially non-covalent *via* intercalation. The binding constants showed that the DNA-binding ability increased in the order of **4** > **2** > **3** > **1**. Competitive binding

studies with EB revealed the ability of the complexes to displace EB from an EB–DNA complex. Cyclic voltammetric and viscosity measurements confirm the intercalative mode of binding of the nickel(II) complex to CT-DNA. CD spectra results indicate that no conformational change in DNA is observed. The interactions between nickel(II) benzhydrazone complexes and BSA in a buffer solution, which were studied by UV-vis, fluorescence and synchronous fluorescence methods, suggest that the complexes possess a strong ability to quench the fluorescence of BSA mainly by a static quenching mechanism. The results of synchronous fluorescence measurements revealed that the present complexes influence the microenvironment around both tyrosine and tryptophan residues in BSA. The binding constants showed that the protein-binding ability increased in the order of **4** > **2** > **3** > **1**. The results for antioxidant activity indicate that all the complexes have almost comparable values against BHA. In addition, all the complexes exhibited significant cytotoxicity against HeLa and MCF-7 cell lines without greatly affecting normal NIH-3T3 cells. Furthermore, fluorescence staining techniques and flow cytometry using the annexin-V assay revealed that complex **4** induces apoptosis in cancer cells.

Acknowledgements

R. R. K. thanks the DST-INSPIRE Program for financial assistance as a JRF (IF130075). We thank UGC-SAP and DST-India (FIST programme) for the use of Bruker 400 MHz NMR, UV-visible and fluorescence spectral facilities at the School of Chemistry, Bharathidasan University. We thank Prof. A. Ramu, Madurai Kamaraj University and Prof. N. Thajuddin, Bharathidasan University, for providing CD and confocal instrumental facilities. We thank Dr Sanjib Karmakar, SAIF, Department of Instrumentation & USIC, Gauhati University, Guwahati for collecting single-crystal X-ray diffraction data. We also thank the CSIR, New Delhi for the electrochemical analyser through research project Ref. No.: 02(0142)/13/EMR-II.

References

1 S. Leininger, B. Olenyuk and P. J. Stang, *Chem. Rev.*, 2000, **100**, 853–908.
2 S. Feng and R. Xu, *Acc. Chem. Res.*, 2001, **34**, 239–247.
3 B. Spingler, C. Da Pieve, A. Medina-Molner, P. M. Antoni and M. G. Santangelo, *Int. J. Chem.*, 2009, **63**, 153–156.
4 G. Zuber, J. C. Quada and S. M. Hecht, *J. Am. Chem. Soc.*, 1998, **120**, 9368–9369.
5 B. Rosenberg, L. van Camp, J. E. Trosko and V. H. Mansour, *Nature*, 1969, **222**, 385–386.
6 B. Rosenberg, L. van Camp and T. Krigas, *Nature*, 1965, **205**, 698–699.
7 J. M. Rademaker-Lakhai, D. van den Bongard, D. Pluim, J. H. Beijnen and J. H. Schellens, *Clin. Cancer Res.*, 2004, **10**, 3717–3727.
8 M. A. Jakupec and B. K. Keppler, *Curr. Top. Med. Chem.*, 2004, **4**, 1575–1583.
9 P. J. Barnard and S. J. Berners-Price, *Coord. Chem. Rev.*, 2007, **251**, 1889–1902.
10 B. P. Espósito and R. Najjar, *Coord. Chem. Rev.*, 2002, **232**, 137–149.
11 J. E. Patterson and D. M. Geller, *Biochem. Biophys. Res. Commun.*, 1977, **74**, 1220–1226.
12 R. T. A. MacGillivray, D. W. Chung and E. W. Davie, *Eur. J. Biochem.*, 1979, **98**, 477–485.
13 K. Hirayama, S. Akashi, M. Furuya and K. Fukuhara, *Biochem. Biophys. Res. Commun.*, 1990, **173**, 639–646.
14 U. Kragh-Hansen, *Pharmacol. Rev.*, 1981, **33**, 17–53.
15 I. Cantuti-Castelvetri, B. Shukitt-Hale and J. A. Joseph, *Int. J. Dev. Neurosci.*, 2000, **18**, 367–381.
16 Y.-J. Surh, K.-S. Chun, H.-H. Cha, S. S. Han, Y.-S. Keum, K.-K. Park and S. S. Lee, *Mutat. Res., Fundam. Mol. Mech. Mutagen.*, 2001, **480–481**, 243–268.
17 J. Vaya and M. Aviram, *Curr. Med. Chem.: Immunol., Endocr. Metab. Agents*, 2001, **1**, 99–117.
18 O. I. Aruoma, *Mutat. Res., Fundam. Mol. Mech. Mutagen.*, 2003, **523–524**, 9–20.
19 K. J. A. Davies, *IUBMB Life*, 2000, **50**, 279–289.
20 A. C. Torbergsen and A. R. Collins, *Eur. J. Nutr.*, 2000, **39**, 80–85.
21 P. K. Singh and D. N. Kumar, *Spectrochim. Acta, Part A*, 2006, **64**, 853–858.
22 B. Singh, R. Srivastava and K. K. Narang, *Synth. React. Inorg. Met.-Org. Chem.*, 2000, **30**, 1175–1192.
23 J. D. Ranford, J. J. Vittal and Y. M. Wang, *Inorg. Chem.*, 1998, **37**, 1226–1231.
24 J. L. Buss, B. T. Greene, J. Turner, F. M. Torti and S. V. Torti, *Curr. Top. Med. Chem.*, 2004, **4**, 1623–1635.
25 P. S. Donnelly, A. Caragounis, T. Du, K. M. Laughton, I. Volitakis, R. A. Cherny, R. A. Sharples, A. F. Hill, Q. X. Li, C. L. Masters, K. J. Barnham and A. R. White, *J. Biol. Chem.*, 2008, **283**, 4568–4577.
26 V. Martin-Diaconescu and M. J. Maroney, in *Comprehensive Inorganic Chemistry II*, ed. J. R. Poeppelmeier, Elsevier, Amsterdam, Second edn, 2013, pp. 295–322, DOI: 10.1016/B978-0-08-097774-4.00319-3.
27 L. Signor, C. Knuppe, R. Hug, B. Schweizer, A. Pfaltz and B. Jaun, *Chem.–Eur. J.*, 2000, **6**, 3508–3516.
28 C. J. Campbell, J. F. Rusling and C. Brückner, *J. Am. Chem. Soc.*, 2000, **122**, 6679–6685.
29 M. P. Sathisha, U. N. Shetti, V. K. Revankar and K. S. R. Pai, *Eur. J. Med. Chem.*, 2008, **43**, 2338–2346.
30 S. M. Pradeepa, H. S. Bhojya Naik, B. Vinay Kumar, K. Indira Priyadarsini, A. Barik and T. R. Ravikumar Naik, *Spectrochim. Acta, Part A*, 2013, **101**, 132–139.
31 S.-Y. Lee, A. Hille, C. Frias, B. Kater, B. Bonitzki, S. Wölfl, H. Scheffler, A. Prokop and R. Gust, *J. Med. Chem.*, 2010, **53**, 6064–6070.
32 H. Wu, J. Yuan, Y. Bai, G. Pan, H. Wang and X. Shu, *J. Photochem. Photobiol., B*, 2012, **107**, 65–72.
33 E. Ramachandran, D. Senthil Raja, N. S. P. Bhuvanesh and K. Natarajan, *Eur. J. Med. Chem.*, 2013, **64**, 179–189.

34 X. Totta, A. A. Papadopoulou, A. G. Hatzidimitriou, A. Papadopoulos and G. Psomas, *J. Inorg. Biochem.*, 2015, **145**, 79–93.
35 P. Krishnamoorthy, P. Sathyadevi, R. R. Butorac, A. H. Cowley, N. S. P. Bhuvanesh and N. Dharmaraj, *Dalton Trans.*, 2012, **41**, 6842–6854.
36 A. R. B. Rao and S. Pal, *J. Organomet. Chem.*, 2011, **696**, 2660–2664.
37 S. Anbu, M. Kandaswamy and B. Varghese, *Dalton Trans.*, 2010, **39**, 3823–3832.
38 *I. M. SADABS: Area-Detector Absorption Correction*, Siemens Industrial Automation, WI, 1996.
39 G. Sheldrick, *Acta Crystallogr., Sect. A: Found. Crystallogr.*, 2008, **64**, 112–122.
40 *W. Bruker-Nonious*, M. Bruker Axs Inc., USA, 2004.
41 P. Lincoln, E. Tuite and B. Nordén, *J. Am. Chem. Soc.*, 1997, **119**, 1454–1455.
42 B. Nordén and F. Tjerneld, *Biopolymers*, 1982, **21**, 1713–1734.
43 J. B. Chaires, N. Dattagupta and D. M. Crothers, *Biochemistry*, 1982, **21**, 3933–3940.
44 G. Cohen and H. Eisenberg, *Biopolymers*, 1969, **8**, 45–55.
45 C. V. Kumar, A. Buranaprapuk, H. C. Sze, S. Jockusch and N. J. Turro, *Proc. Natl. Acad. Sci. U. S. A.*, 2002, **99**, 5810–5815.
46 M. S. Blois, *Nature*, 1958, **181**, 1199–1200.
47 T. Nash, *Biochem. J.*, 1953, **55**, 416–421.
48 L. C. Green, D. A. Wagner, J. Glogowski, P. L. Skipper, J. S. Wishnok and S. R. Tannenbaum, *Anal. Biochem.*, 1982, **126**, 131–138.
49 T. Mosmann, *J. Immunol. Methods*, 1983, **65**, 55–63.
50 G. Repetto, A. del Peso and J. L. Zurita, *Nat. Protoc.*, 2008, **3**, 1125–1131.
51 I. Vermes, C. Haanen, H. Steffens-Nakken and C. Reutellingsperger, *J. Immunol. Methods*, 1995, **184**, 39–51.
52 L. J. Ackerman, P. E. Fanwick, M. A. Green, E. John, W. E. Running, J. K. Swearingen, J. W. Webb and D. X. West, *Polyhedron*, 1999, **18**, 2759–2767.
53 R. Raveendran and S. Pal, *J. Organomet. Chem.*, 2007, **692**, 824–830.
54 M. Sönmez, A. Levent and M. Şekerci, *Russ. J. Coord. Chem.*, 2004, **30**, 655–660.
55 N. Selvakumaran, A. Pratheepkumar, S. W. Ng, E. R. T. Tiekink and R. Karvembu, *Inorg. Chim. Acta*, 2013, **404**, 82–87.
56 K. Mitra, S. Biswas, C. R. Lucas and B. Adhikary, *Inorg. Chim. Acta*, 2006, **359**, 1997–2003.
57 Y. Kurt, A. Koca, M. Akkurt and B. Ülküseven, *Inorg. Chim. Acta*, 2012, **388**, 148–156.
58 S. V. Kryatov, B. S. Mohanraj, V. V. Tarasov, O. P. Kryatova, E. V. Rybak-Akimova, B. Nuthakki, J. F. Rusling, R. J. Staples and A. Y. Nazarenko, *Inorg. Chem.*, 2002, **41**, 923–930.
59 C. Hansch, A. Leo and R. W. Taft, *Chem. Rev.*, 1991, **91**, 165–195.
60 D. Senthil Raja, N. S. P. Bhuvanesh and K. Natarajan, *Inorg. Chem.*, 2011, **50**, 12852–12866.
61 V. Uma, M. Kanthimathi, T. Weyhermuller and B. U. Nair, *J. Inorg. Biochem.*, 2005, **99**, 2299–2307.
62 X.-L. Wang, H. Chao, H. Li, X.-L. Hong, Y.-J. Liu, L.-F. Tan and L.-N. Ji, *J. Inorg. Biochem.*, 2004, **98**, 1143–1150.
63 C. Tan, J. Liu, L. Chen, S. Shi and L. Ji, *J. Inorg. Biochem.*, 2008, **102**, 1644–1653.
64 M. T. Carter, M. Rodriguez and A. J. Bard, *J. Am. Chem. Soc.*, 1989, **111**, 8901–8911.
65 S.-S. Zhang, S.-Y. Niu, B. Qu, G.-F. Jie, H. Xu and C.-F. Ding, *J. Inorg. Biochem.*, 2005, **99**, 2340–2347.
66 Y. Ni, D. Lin and S. Kokot, *Anal. Biochem.*, 2006, **352**, 231–242.
67 H. Liu, L. Li, Q. Guo, J. Dong and J. Li, *Transition Met. Chem.*, 2013, **38**, 441–448.
68 S. Satyanarayana, J. C. Dabrowiak and J. B. Chaires, *Biochemistry*, 1992, **31**, 9319–9324.
69 S. Satyanarayana, J. C. Dabrowiak and J. B. Chaires, *Biochemistry*, 1993, **32**, 2573–2584.
70 X. Z. H. G. Z. Zen, J. G. Xu, Z. Z. Zheng and Z. B. Wang, *Methods of Fluorescence Analysis*, Science press, Beiging, 2 edn, 1990.
71 C. W. Fuller and J. N. Miller, *Proc. Anal. Div. Chem. Soc.*, 1979, **16**, 199–208.
72 T. N. Parac and N. M. Kostić, *J. Am. Chem. Soc.*, 1996, **118**, 51–58.
73 Z. Afrasiabi, E. Sinn, S. Padhye, S. Dutta, S. Padhye, C. Newton, C. E. Anson and A. K. Powell, *J. Inorg. Biochem.*, 2003, **95**, 306–314.
74 P. Sathyadevi, P. Krishnamoorthy, R. R. Butorac, A. H. Cowley, N. S. P. Bhuvanesh and N. Dharmaraj, *Dalton Trans.*, 2011, **40**, 9690–9702.

